

Chirality Driven by Magnetic Dipole Response for Demultiplexing of Surface Waves


Ivan S. Sinev,* Andrey A. Bogdanov, Filipp E. Komissarenko, Kristina S. Frizyuk, Mihail I. Petrov, Ivan S. Mukhin, Sergey V. Makarov, Anton K. Samusev, Andrei V. Lavrinenko, and Ivan V. Iorsh

Surface electromagnetic waves are characterized by the intrinsic spin-orbit interaction which results in the fascinating spin-momentum locking. Therefore, directional coupling of light to surface waves can be achieved through chiral nanoantennas. Here, we show that dielectric nanoantenna provides chiral response with strong spectral dependence due to the interference of electric and magnetic dipole momenta when placed in the vicinity of the metal-air interface. Remarkably, chiral behaviour in the proposed scheme does not require elliptical polarization of the pump beam or the geometric chirality of the nanoantenna. We show that the proposed ultracompact and simple dielectric nanoantenna allows for both directional launching of surface plasmon polaritons on a thin gold film and their demultiplexing with a high spectral resolution.

1. Introduction

Metal surfaces,^[1,2] metasurfaces,^[3–6] and 2D materials^[7–9] provide means to support surface waves with tailorable polarization states, which fit perfectly into the emerging field of on-chip optical communications. One of the most fascinating properties of the surface waves is their intrinsic spin-momentum locking^[10] which rigidly connects the direction of propagation of the surface wave and its transverse spin angular momentum.^[11] This property opens appealing possibilities in the fields of nano-optomechanics,^[12] routing of surface electromagnetic waves^[13] and quantum nanophotonics.^[14] The essence of the effect is that an emitter characterized by circular polarization of certain helicity will excite a surface wave with a certain propagation direction.

I. S. Sinev, A. A. Bogdanov, F. E. Komissarenko, K. S. Frizyuk, M. I. Petrov, I. S. Mukhin, S. V. Makarov, A. K. Samusev, A. V. Lavrinenko, I. V. Iorsh
ITMO University
St. Petersburg 197101, Russia
E-mail: i.sinev@metalab.ifmo.ru
F. E. Komissarenko, I. S. Mukhin
St. Petersburg Academic University
St. Petersburg 194021, Russia
A. V. Lavrinenko
Technical University of Denmark
Kongens Lyngby, Denmark

 The ORCID identification number(s) for the author(s) of this article can be found under <https://doi.org/10.1002/lpor.201700168>

DOI: 10.1002/lpor.201700168

The chiral response is usually achieved either by breaking the time-reversal symmetry of the two-level system with magnetic fields^[15] for the case of quantum emitters, by using elliptically polarized pump fields^[13,16] or by the geometric chirality for the case of classical scatterers.

There is an alternative way to achieve effective circular electric polarizability of the emitter by exploiting the magnetic dipole. In this case the phase delay between the electric and magnetic dipole response lead to the emergence of the effective elliptical electric polarization of the emitter providing the required chirality. The crucial condition is the comparable oscillator strength of the electric and magnetic dipole transitions. For the

quantum emitters such as quantum dots and individual atoms this is hardly fulfillable since the magnetic dipole transitions are suppressed as compared to the electric dipole ones.

There is, however, a classical nanoscatterer which readily provides comparable magnetic and electric responses: a high-index dielectric nanoantenna.^[17–19] Due to strong displacement currents induced in the volume of the high-index dielectric particle, its effective magnetic polarizability can reach amplitudes comparable or even stronger than that of electric polarizability.^[17,20,21] Furthermore, the spectral position and relative strength of electric and magnetic optical resonances can also be independently tailored by changing the shape of the nanoparticle, which can lead to a plethora of fascinating effects, like directional scattering,^[22–26] generalized Brewster effect,^[27] *etc.*^[19] However, up to now the studies of high-index nanoparticles have been mainly focused on their applications for manipulation of bulk waves, while their performance for launching surface waves remained mostly unexplored, with only a few papers addressing this problem theoretically.^[28–30]

Here, we experimentally demonstrate that a very basic dielectric nanoantenna, a single silicon nanosphere, provides chiral response with a strong spectral dependence. Therefore, it can serve as a highly efficient and ultracompact source and demultiplexer for surface waves with a high spectral resolution (<50 nm) and opposite propagation directions of the demultiplexed waves. We show that the inherently strong magnetic dipole response of the silicon particle provides extremely efficient excitation of a SPP wave, whereas mutual interference of the electric and

magnetic dipole resonances of the nanoantenna provides high front-to-back ratio contrast and directivity values for the excited surface waves. As a result, dielectric nanoantenna holds a major advantage over previously proposed SPP demultiplexer designs, offering both extreme compactness as compared to grating structures^[31–33] and decisively superior spectral resolution as compared to other subwavelength demultiplexer solutions.^[34–37] The theoretical framework that we formulate to describe the physics behind the observed phenomena can be easily extended to more complex interfaces supporting other types of surface waves.^[5,6] The combination of dispersion engineering of states supported by a 2D interface and tunability of the nanoantenna radiation pattern would be an important step forward to efficient routing of surface waves. Moreover, the proposed approach could be directly mapped to the quantum photonic set-ups: in this case the dielectric nanoantenna should be substituted with a quantum dot or an atom with a resonantly enhanced magnetic dipole and suppressed electric dipole transitions. This would open new routes in the rapidly evolving field of the chiral quantum optics.

Methods

Sample Fabrication

Silicon nanospheres were fabricated from a thin silicon film on the glass substrate using the femtosecond laser ablation method.^[38,39] After that, nanospheres with diameters ranging from 250 to 310 nm were transferred to a thin (40 nm) gold film on the glass substrate by nanomanipulations under an electron beam.^[40] This method allows for precise positioning of nanospheres in clear regions of the substrate far from other defects, that ensures extremely low parasitic scattering of the SPPs.

Experiment

To visualize the directivity patterns of SPPs excited on a thin gold film by a single silicon nanosphere using a leakage radiation microscopy (LRM) setup combined with Fourier plane imaging optics^[41–44] (for details of the setup see Supplementary Material). In the LRM experiments, a SPP from a single silicon nanosphere was excited with an obliquely incident TM-polarized beam mildly focused on the nanosphere with an achromatic doublet lens, which ensured good trade-off between the SPP excitation efficiency and angular divergence of the excitation beam. The SPP radiation leaking through the thin gold film was then collected from the bottom with an oil immersion objective. For tracking the spectral evolution of the SPP directivity patterns, we used supercontinuum white light source (Fianium White-Lase SC400-6) combined with acousto-optic tunable filter (Fianium AOTF) yielding a narrowband (≈ 4 nm) beam with the tunable central wavelength within the visible to near-infrared regions (650–1100 nm). To provide a smooth Gaussian beam profile required for accurate measurement of Fourier plane images, the beam was spatially filtered with a single-mode fiber. Since the data provided by the Fourier plane image represent the angular spectrum of the SPP leakage radiation, it offers a simple and di-

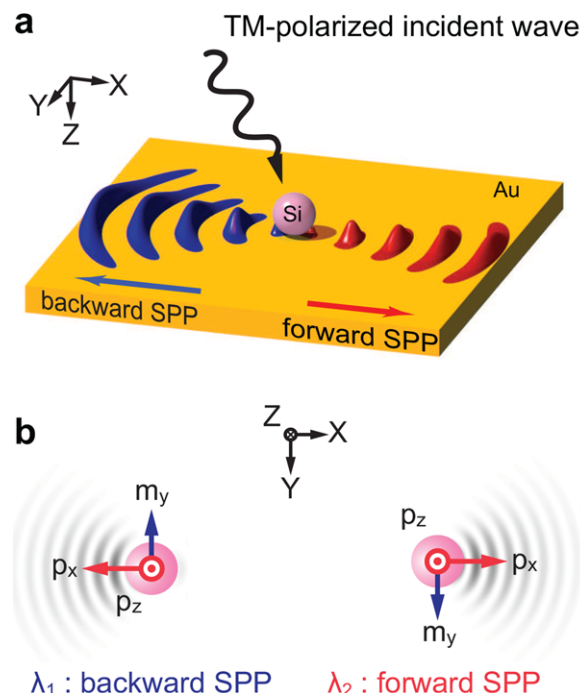


Figure 1. Regimes of SPP generation by a silicon nanosphere excited with polarized light at oblique incidence. Note that only the dipole moments induced in the sphere that contribute to SPP excitation are shown.

rect way of reconstructing the full SPP directivity pattern. This is achieved by plotting the radial dependence of the intensity of light coming from the sample at an angle corresponding to the direction of SPP leakage radiation, which in the Fourier image forms a well-defined double-crescent shape (see Figure 3a).

2. Results

2.1. Theoretical Concept

To study surface plasmon polaritons excited by a silicon nanosphere, we employ the analytical model based on the Green function approach.^[45] This model relies on calculation of the sphere electric and magnetic polarizabilities in the dipole approximation. Applicability of the dipole approximation for calculation of plasmon fields was discussed in Ref. ^[46]. Due to the structure of SPP fields,^[1] the only dipole component that does not couple to a SPP mode is the normal magnetic one. Therefore, for the s-polarized excitation the SPP directivity pattern is inherently symmetric. The p-polarized excitation, on the other hand, can provide directional excitation of a SPP due to interference between the induced dipole moments (see Figure 1), as it is devised in the following.

In the case of a p-polarized wave, three independent dipole moments are excited in the silicon nanosphere: magnetic dipole along the y axis, characterized by magnetic polarizability m_y and two electric dipoles along the z and x axes with polarizabilities p_z and p_x , respectively (see scheme in Figure 1b). Notably, polarizabilities m_y , p_z , p_x differ substantially from those of a silicon nanosphere in vacuum due to bianisotropy induced by the

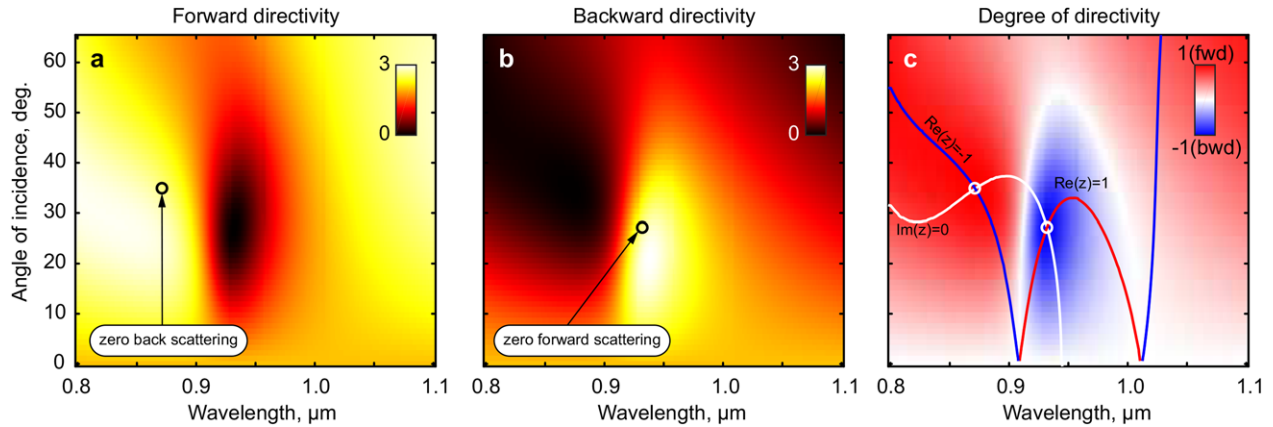


Figure 2. Analytically calculated maps of (a) forward directivity, (b) backward directivity and (c) degree of directivity of surface plasmon polariton launched by a single 297 nm silicon nanosphere on the gold substrate. The SPP direction is given with respect to the direction of the in-plane component of the wavevector of the incident plane wave. In panel (c), the isolines for the real and imaginary parts of parameter z characterizing the SPP directivity illustrate the regimes of complete cancellation of forward or backward SPP scattering at the intersections of $Re(z) = \pm 1$ curves with $Im(z) = 0$ curve, which are marked with circles in all three panels.

substrate as discussed in Refs. [45,47]. The magnetic field produced by these point dipoles can be written as

$$\mathbf{H}(\mathbf{r}) = k_0^2 G_H(\mathbf{r}) \mathbf{m} + i k_0 \nabla \times G_E(\mathbf{r}) \mathbf{p}, \quad (1)$$

where $\mathbf{r} = (\rho, \phi_0, 0)$ is the radius vector in the plane of the interface in cylindrical coordinates, $k_0 = \omega/c$, and G_H, G_E are the total magnetic and electric Green functions for the dipole above the metallic substrate. The Green functions can be separated into the bare and reflected parts, the latter being solely responsible for the surface plasmon contribution. By writing the explicit form of the reflected parts of the Green functions as a two-dimensional Fourier transform and simplifying the equations using asymptotic relations (see Supplementary Material for details) we arrive at the following equation for the SPP magnetic field vector in the Cartesian basis:

$$\mathbf{H}_{SPP} \sim \frac{e^{ik_{SPP}\rho}}{\sqrt{\rho}} \begin{pmatrix} \frac{1}{2} \sin 2\phi_0 (m_y - \tilde{k}_z p_x) + \tilde{k}_{SPP} \sin \phi_0 \\ \cos^2 \phi_0 (m_y - \tilde{k}_z p_x) - \tilde{k}_{SPP} \cos \phi_0 \\ 0 \end{pmatrix}. \quad (2)$$

Here, $\tilde{k}_{SPP} = k_{SPP}/k_0 = \sqrt{\epsilon_m/(\epsilon_m + 1)}$, $\tilde{k}_z = \sqrt{1 - \tilde{k}_{SPP}^2} = \sqrt{1/(\epsilon_m + 1)}$, and ϵ_m is the dielectric permittivity of the metal. The intensity of SPP launched by the nanosphere in a given direction is proportional to $|H_\phi|^2$, where $H_\phi = H_y \cos \phi_0 - H_x \sin \phi_0$. We thus obtain the expression for the SPP field intensity in a given direction:

$$I_{SPP} \sim \frac{1}{\rho} |\cos \phi_0 (m_y - i\kappa p_x) - \tilde{k}_{SPP} p_z|^2, \quad (3)$$

where $\kappa = -i\tilde{k}_z$. It is convenient to introduce the complex dimensionless parameter $z = (m_y - i\kappa p_x)/(\tilde{k}_{SPP} p_z)$. Then, the azimuthal dependence of the plasmon intensity can be written as:

$$I_{SPP}(\phi_0) \sim (1 - \text{Re}z \cos \phi_0)^2 + (\text{Im}z)^2 \cos^2 \phi_0. \quad (4)$$

This expression has two important consequences. First, it can be shown that the maximal achievable directivity $D(\phi_0) = 2\pi I_{SPP}(\phi_0)/\int d\phi I_{SPP}(\phi)$ is equal to 3. Second, unlike the case of non-active nanoantennas for bulk waves,^[48,49] both forward or backward scattering of the incident light into SPPs can be totally suppressed, if condition $z = \pm 1$ is satisfied.

The central theoretical expression of the paper, Eq. (4) also grasps the physics behind the conventional chiral plasmonic devices. Namely, if the magnetic response of the scatterer vanishes we can write z simply as $-i\kappa p_x/(\tilde{k}_{SPP} p_z)$. Thus, directional excitation of the surface plasmon can be achieved if and only if $\text{Im}(p_x/p_z) \neq 0$, i.e. there is a phase delay between two electric polarization projections, which can be achieved either through elliptical polarization of the incident field or by using the geometric chirality of the scatterer. The condition $z = \pm 1$ can also be considered as an extension of the null-scattering Kerker conditions^[49] to the domain of surface waves. Namely, in the long wavelength limit ($\kappa = 0, k_{SPP} = 1$) $z = \pm 1$ is reduced to the well-known Kerker conditions for free space scattering $m_y = \pm p_z$.

Remarkably, these fascinating effects are readily available for the simplest example of a dielectric nanoantenna, spherical nanoparticle, under linearly polarized illumination. This is illustrated in **Figure 2** for a 297 nm silicon nanosphere on gold substrate. The maps of forward and backward directivity shown in **Figure 2 a,b** in the “wavelength-angle of incidence” axes reveal resonant suppression of forward SPP and respective increase of the backward SPP at around 935 nm. Importantly, for the presented spectral range and angles of incidence the conditions for total suppression of backward and forward scattering are independently fulfilled. This is best illustrated in **Figure 2c**, where the map of the degree of directivity (DOD) is presented. We define this value as $\text{DOD} = (I_f - I_b)/(I_f + I_b)$, where I_f and I_b stand for the SPP intensity in the forward and backward directions, respectively. Following Eq.(4), the exact excitation conditions for total cancellation of backward ($\text{DOD}=1$) and forward ($\text{DOD}=-1$) SPPs can be found as the intersections of $\text{Im}(z) = 0$ isoline with either $\text{Re}(z) = -1$ or $\text{Re}(z) = 1$ isolines, which are also shown in **Figure 2c**. The relevant intersection points are marked with

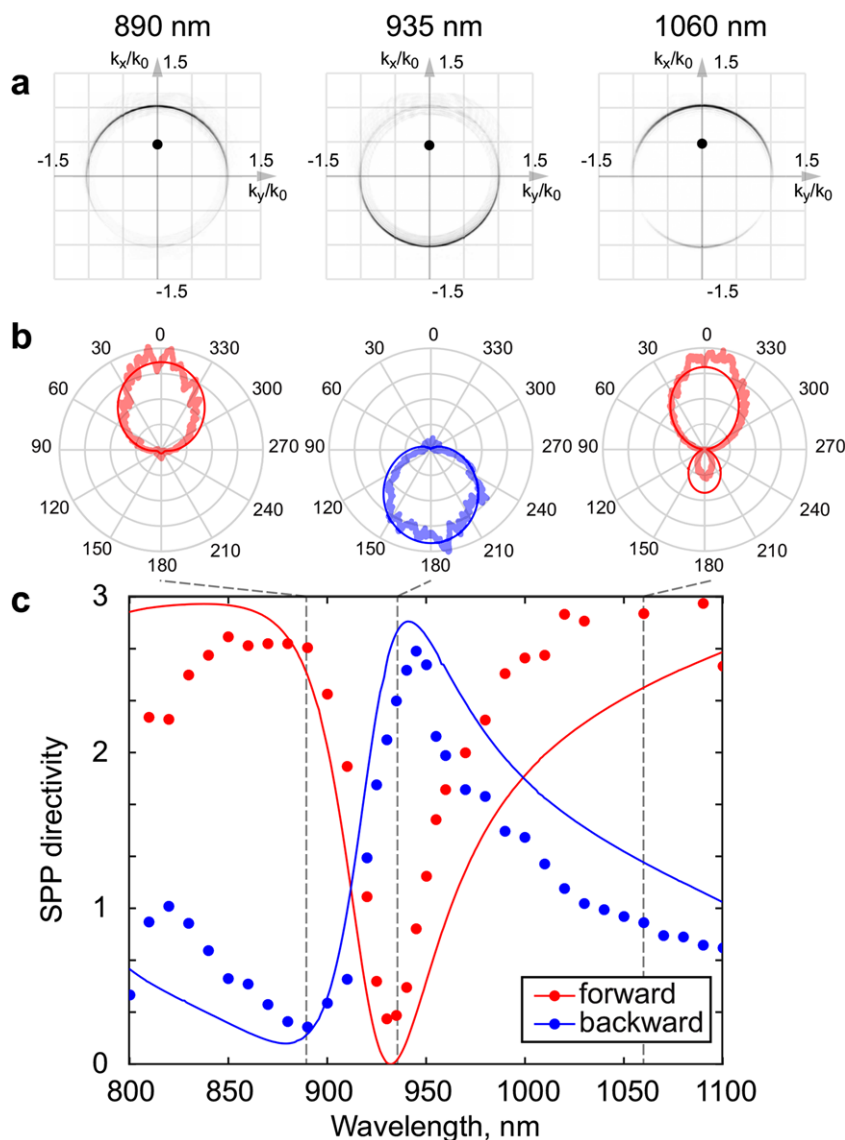


Figure 3. Experimental demonstration of switching of SPP radiation patterns by a silicon nanoantenna. (a) (False color) Fourier plane images of SPP launched by a ≈ 295 nm silicon nanosphere on 40 nm gold film for 890, 935 and 1060 nm excitation wavelengths. Small black circles mark the angular range of the excitation radiation which is incident at around 25 degrees. (b) SPP directivity patterns reconstructed from the measured Fourier images (thick lines) and analytically calculated directivity patterns (thin lines). (c) Spectral dependence of the forward and backward SPP intensity demonstrating efficient switching between the SPP excitation directions. Experimental data (dots) and analytical data for a 297 nm silicon sphere on the gold substrate are shown. The wavelengths corresponding to data presented in (a,b) are marked with dashed lines.

circles in Figure 2a-c. It is also worth noting that the conditions for zero forward/backward SPP scattering do not correspond to maximum SPP directivity, as shown in Figure 2a,b. While the exact conditions for achieving maximum directivity can be derived from eq. 3, they are extremely cumbersome due to substrate-induced renormalization of the particle polarizability.

2.2. Experimental Results

To confirm the SPP directivity switching experimentally, we visualized the directivity patterns of SPPs excited on a thin gold film by a single silicon nanosphere using a leakage radiation

microscopy (LRM) setup combined with Fourier plane imaging optics^[41–44] (for details see Methods and Supplementary Material). Here, we focused on the observation of the regime of forward SPP scattering cancellation, since it is a crucial feature of our system. Therefore, the angle of incidence of a p-polarized beam was chosen to be 25 degrees, which allows the fulfillment of condition $z = 1$ according to the analytical model (see Figure 2c). Figure 3a,b show the Fourier plane images and reconstructed directivity patterns of SPPs from a single silicon nanosphere ($d \approx 295$ nm) for three distinctive regimes at characteristic excitation wavelengths: highly directional forward scattering (890 nm), inversion of the directivity pattern at 935 nm, and recovery of forward scattering at 1060 nm. The resonant behavior of the

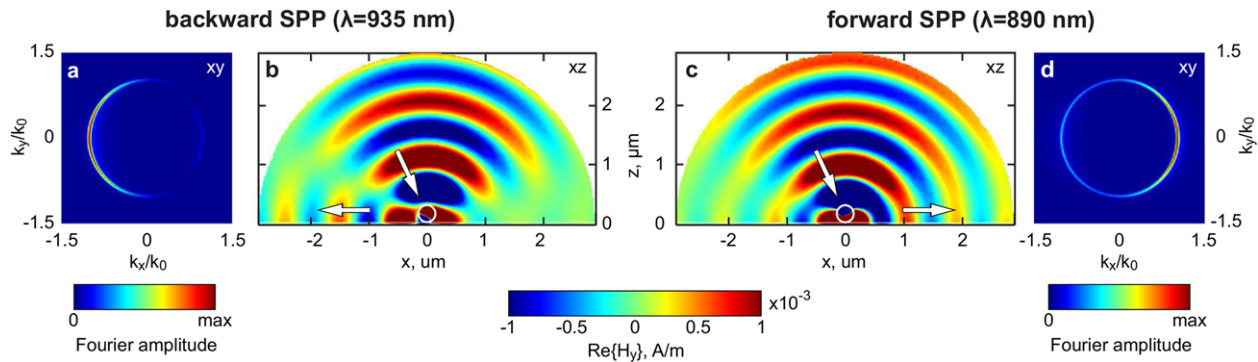


Figure 4. Numerical calculations illustrating the backward (a,b), $\lambda=935$ nm and forward (c,d), $\lambda=890$ nm, SPP excitation regimes by a 290 nm silicon nanosphere on 40 nm gold film excited by a plane wave incident at 25 degrees to the substrate surface. (b) and (c) show the sections of the scattered magnetic field (H_y) in the plane of incidence (xz). The directions of the incident plane wave and the SPP launched by the sphere are shown with arrows. (a) and (d) show the Fourier transforms of the calculated SPP fields in the substrate plane (xy) illustrating the directivity of the excited SPPs.

switching process is illustrated in Figure 3c, where the spectral dependence of the SPP directivity in the forward and backward directions is shown. These results are in excellent agreement with the analytical calculations of the SPP directivity performed using Eq.(3) for a 297 nm silicon nanosphere, which are shown in Figure 3c with thin lines. The sphere diameter in the calculations was chosen for the best matching of the spectral position of forward SPP directivity dip near 935 nm. Note that unlike the analytical data, the measured minimum forward plasmon intensity does not reach zero due to the angular divergence and non-monochromaticity of the incident beam. Despite this, we readily observe switching of front-to-back ratio of SPP excitation from 11 to 0.13 within less than 50 nm spectral band (890 to 935 nm). The full spectral dependence of the measured Fourier plane images for the 295 nm nanosphere is shown in Supplementary Movie S1. The difference in SPP demultiplexing bandwidth between the experimental data and analytical calculations observed in Figure 3c could be concerned with the deviations of the fabricated silicon nanoparticle shape from ideal sphere.

2.3. Discussion

We also illustrate the demultiplexing of SPPs and the applicability of the dipole approximation with full wave numerical calculations of the electromagnetic fields distribution near the silicon nanoantenna on the gold film in COMSOL Multiphysics package. The results of the simulations for the backward ($\lambda=935$ nm) and forward ($\lambda=890$ nm) SPP excitation regimes for 25° angle of incidence are presented in Figure 4. The maps of the scattered magnetic field distribution in the plane (Figure 4b,c) unambiguously show the switching of the SPP direction. This is further supported by the Fourier transform of the SPP fields presented in Figure 4a,d (see Supplementary Material), which perfectly reproduce the experimental leakage radiation images (Figure 3). Note that in numerical simulations the best matching of the SPP reversal condition to the experimental data was achieved for the sphere diameter of 290 nm, which slightly differs from the sphere diameter in analytical model (297 nm). Time evolution of the scattered magnetic field profiles in forward and backward SPP excitation

regimes are illustrated in Supplementary Movies S2 and S3, respectively.

Another major advantage of using dielectric nanoantennas for excitation of SPPs is the scalability of their resonances and, consequently, the spectral position of the resonant cancellation of forward scattering. This is illustrated in Figure 5a, where the experimental spectra of the forward SPP directivity is shown for four silicon nanospheres of different diameters ranging from 250 to 310 nm. Therefore, simply by changing the nanoparticle size, which can be controlled with high precision in modern laser ablation techniques,^[38] resonant inversion of the SPP excitation pattern can be tuned within a broad spectral range from visible to infrared frequencies. High spectral resolution of switching could also open the path for reconfigurable demultiplexing devices, for example, based on antennas with tunable refractive index,^[50] thus extending the idea of programmable metasurfaces^[51] to devices operating with surface waves.

Moreover, the directional excitation of SPPs with dielectric nanoparticles is extremely efficient due to their strong magnetic dipole response. The expression for the SPP intensity (see Eq.(3)) shows that the contribution of the lateral electric dipole moment to SPP excitation is suppressed by a factor of $1/\kappa \sim \sqrt{\epsilon_m + 1}$ as compared to the contribution of lateral magnetic dipole moment. For the SPP on gold in the near-infrared spectral range, this ratio can reach values of 5-7.^[52] To provide quantitative estimation of the SPP excitation efficiency, we compare the cross sections of scattering of plane waves into SPPs for gold and silicon nanoparticles of the same size. While silicon nanoparticles possess an inherently strong magnetic dipole response, the gold nanoparticles gain one only due to interaction with the gold substrate via the bianisotropy mechanism,^[45] and it is still weak as compared to the electric dipole moment. Spectral dependences of SPP excitation efficiency for gold and silicon nanospheres are compared in Figure 5b. It shows the cross sections of scattering into SPP for gold and silicon nanospheres of the same size calculated for normal incidence and normalized to the physical cross sections of the nanoparticles. The results of both numerical and analytical calculations are shown. The presented data confirm the expected superior performance of silicon nanoparticles for excitation of SPPs and reveal the spectral range of applicability of the point dipole approximation. The maximum cross section of scattering

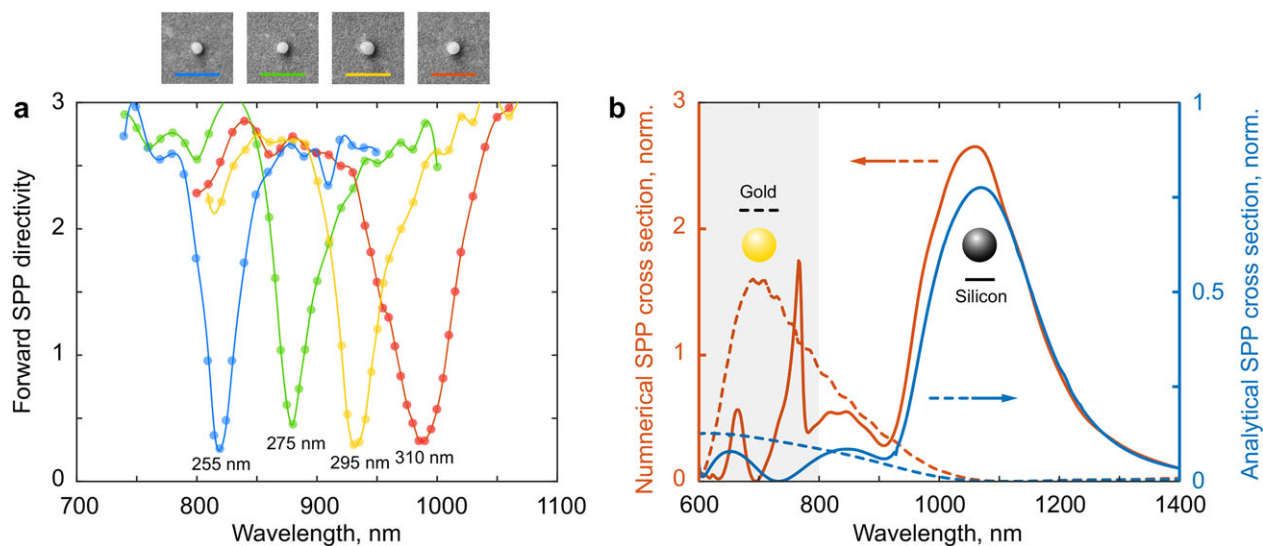


Figure 5. (a) Experimentally measured spectra of forward SPP directivity for four silicon nanospheres of different diameters showing the scalability of the SPP switching condition. The inset shows SEM images of the particles in the order of increasing the wavelength of the measured forward SPP directivity dip. This is additionally encoded with the color of the scale bars which represent 1 μm . The approximate sizes of the nanoparticles marked in the plot are obtained via fitting the spectra with the analytical model (not shown). (b) Calculated scattering cross sections into SPP for silicon (solid lines) and gold (dashed lines) nanoparticles of the same sizes reveals superior SPP excitation efficiency by a silicon nanoparticle. The results of numerical model (red lines, sphere diameter 290 nm) and analytical calculation within dipole approximation (blue lines, sphere diameter 297 nm) are compared. The cross sections are calculated for normally incident plane wave excitation and are normalized to the physical section of the particles. The shaded area shows the spectral region of excitation of higher order multipole modes, where the analytical model is not applicable.

into SPP, which is reached in the vicinity of magnetic dipole resonance, is of the same order as the physical cross-section of the nanoparticle, thus comprising a significant fraction of its optical response (see Supplementary Figure S1 for comparison between different contributions to the total extinction cross section). Importantly, Figure 5b also reveals that the analytical model based on the dipole approximation, while accurately reproducing the spectral dependence of SPP excitation efficiency, underestimates its absolute value. This inconsistency is due to the fact that in analytical calculations, we set the point dipole with modified polarizability to the center of the sphere as it is usually done in theoretical studies.^[29,45] However, when the particle is placed on gold substrate, the fields become mainly concentrated near the metal surface.^[47] Therefore, the effective position of the dipole moment should also be closer to the metal surface, which increases the efficiency of coupling to SPP mode. This effect is especially relevant for gold nanoparticle, when the fields are mostly concentrated in the gap between nanoparticle and substrate. For larger angles of incidence this effect is further increased due to additional field enhancement concerned with normal electric dipole mode.^[47] For comparison of SPP excitation efficiencies at oblique incidence, see Supplementary Figure S2.

3. Conclusions and Outlook

To conclude, we have revealed huge potential of high-index dielectric nanoantennas for directional excitation of surface waves and their highly efficient demultiplexing. We have experimentally demonstrated resonant switching between forward and backward excitation of surface plasmon polariton modes within a

narrow spectral band (less than 50 nm) by a single silicon nanosphere. We showed that mutual interference of magnetic and electric dipole moments of the nanosphere provides spectrally dependent chiral response of the nanoantenna, which leads to complete suppression of forward or backward surface waves for different excitation conditions. By merit of scalability of optical resonances of dielectric nanoantennas, these regimes can be tuned within a broad spectral range from visible to infrared. We also showed that the strong magnetic dipole response of a silicon nanosphere provides a superior surface plasmon polariton excitation efficiency, which can not be reached with metallic nanospheres for small angles of incidence. Importantly, the demultiplexing nanoantennas can be fabricated by low-cost and simple laser printing technique, which allows for fast and precise nanosphere deposition on any surface, including predesigned metasurfaces and 2D materials. Keeping in mind that the resonant switching takes place at relatively small angles of incidence of the impinging beam (25°), our findings have important practical implications for on-chip optical communications and surface photonics.

Supporting Information

Supporting Information is available from the Wiley Online Library or from the author.

Acknowledgement

Analytical calculations, sample fabrication, back focal plane measurements, and data processing were financially supported by Russian Science Foundation, grant no. 15-12-20028.

Numerical simulations were funded by the Ministry of Education and Science of Russian Federation (3.8891.2017/8.9).

The authors thank Andrey Evlyukhin and Osamu Takayama for fruitful discussions.

Additional Content

Supporting Information Available: Details of the theoretical analysis, details of the leakage radiation microscopy setup, extraction SPP directivity from numerical calculations, analysis of SPP excitation efficiency for oblique incidence, movies with spectral evolution of the measured SPP directivity patterns and movies of magnetic field scattered by the silicon nanoparticle placed on a gold substrate for two regimes of SPP generation.

Conflict of Interest

The authors have declared no conflict of interest.

Keywords

Dielectric nanoantennas, Chirality, Plasmonics, Silicon, Wavelength demultiplexing

Received: June 19, 2017

Revised: August 3, 2017

Published online: September 11, 2017

- [1] H. Raether, *Surface plasmons on smooth surfaces* (Springer, 1988).
- [2] S. Kitson, W. L. Barnes, and J. Sambles, *Physical Review Letters* **77**(13), 2670 (1996).
- [3] W. A. Murray and W. L. Barnes, *Advanced Materials* **19**(22), 3771–3782 (2007).
- [4] I. I. Smolyaninov, Y. J. Hung, and C. C. Davis, *Science* **315**(5819), 1699–1701 (2007).
- [5] A. A. High, R. C. Devlin, A. Dibos, M. Polking, D. S. Wild, J. Perczel, N. P. de Leon, M. D. Lukin, and H. Park, *Nature* **522**(7555), 192–196 (2015).
- [6] O. Yermakov, A. Ovcharenko, M. Song, A. Bogdanov, I. Iorsh, and Y. S. Kivshar, *Physical Review B* **91**(23), 235423 (2015).
- [7] A. Grigorenko, M. Polini, and K. Novoselov, *Nature Photonics* **6**(11), 749–758 (2012).
- [8] F. Xia, H. Wang, D. Xiao, M. Dubey, and A. Ramasubramaniam, *Nature Photonics* **8**(12), 899–907 (2014).
- [9] D. Basov, M. Fogler, and F. G. de Abajo, *Science* **354**(6309), aag1992 (2016).
- [10] K. Y. Bliokh, F. Rodríguez-Fortuño, F. Nori, and A. V. Zayats, *Nature Photonics* **9**(12), 796–808 (2015).
- [11] K. Y. Bliokh, D. Smirnova, and F. Nori, *Science* **348**(6242), 1448–1451 (2015).
- [12] F. J. Rodríguez-Fortuño, N. Engheta, A. Martínez, and A. V. Zayats, *Nature Communications* **6**, 8799 (2015).
- [13] F. J. Rodríguez-Fortuño, G. Marino, P. Ginzburg, D. O'Connor, A. Martínez, G. A. Wurtz, and A. V. Zayats, *Science* **340**(6130), 328–330 (2013).
- [14] P. Lodahl, S. Mahmoodian, S. Stobbe, A. Rauschenbeutel, P. Schneeweiss, J. Volz, H. Pichler, and P. Zoller, *Nature* **541**(7638), 473–480 (2017).
- [15] R. J. Coles, D. M. Price, J. E. Dixon, B. Royall, E. Clarke, P. Kok, M. S. Skolnick, A. M. Fox, and M. N. Makhonin, *Nature Communications* **7**, 11183 (2016).
- [16] F. J. Rodríguez-Fortuño, I. Barber-Sanz, D. Puerto, A. Griol, and A. Martínez, *ACS Photonics* **1**(9), 762–767 (2014).
- [17] A. I. Kuznetsov, A. E. Miroshnichenko, Y. H. Fu, J. Zhang, and B. Luk'yanchuk, *Scientific Reports* **2**, 492 (2012).
- [18] A. B. Evlyukhin, S. M. Novikov, U. Zywietz, R. L. Eriksen, C. Reinhardt, S. I. Bozhevolnyi, and B. N. Chichkov, *Nano Letters* **12**(7), 3749–3755 (2012).
- [19] A. I. Kuznetsov, A. E. Miroshnichenko, M. L. Brongersma, Y. S. Kivshar, and B. Luk'yanchuk, *Science* **354**(6314), aag2472 (2016).
- [20] R. Fenollosa, F. Meseguer, and M. Tymczenko, *Advanced Materials* **20**(1), 95–98 (2008).
- [21] E. Xifré-Pérez, R. Fenollosa, and F. Meseguer, *Optics Express* **19**(4), 3455–3463 (2011).
- [22] J. M. Geffrin, B. García-Cámara, R. Gómez-Medina, P. Albella, L. Froufe-Pérez, C. Eyraud, A. Litman, R. Vaillon, F. González, M. Nieto-Vesperinas et al., *Nature communications* **3**, 1171 (2012).
- [23] Y. H. Fu, A. I. Kuznetsov, A. E. Miroshnichenko, Y. F. Yu, and B. Luk'yanchuk, *Nature Communications* **4**, 1527 (2013).
- [24] S. Person, M. Jain, Z. Lapin, J. J. Sáenz, G. Wicks, and L. Novotny, *Nano Letters* **13**(4), 1806–1809 (2013).
- [25] Y. F. Yu, A. Y. Zhu, R. Paniagua-Domínguez, Y. H. Fu, B. Luk'yanchuk, and A. I. Kuznetsov, *Laser & Photonics Reviews* **9**(4), 412–418 (2015).
- [26] M. Decker, I. Staude, M. Falkner, J. Dominguez, D. N. Neshev, I. Brener, T. Pertsch, and Y. S. Kivshar, *Advanced Optical Materials* **3**(6), 813–820 (2015).
- [27] R. Paniagua-Domínguez, Y. F. Yu, A. E. Miroshnichenko, L. A. Krivitsky, Y. H. Fu, V. Valuckas, L. Gonzaga, Y. T. Toh, A. Y. S. Kay, B. Luk'yanchuk, and A. I. Kuznetsov, *Nature Communications* **7**, 10362 (2016).
- [28] A. B. Evlyukhin and S. I. Bozhevolnyi, *JETP Letters* **83**(12), 558–562 (2006).
- [29] A. B. Evlyukhin and S. I. Bozhevolnyi, *Physical Review B* **92**(24), 245419 (2015).
- [30] S. V. Li, A. E. Krasnok, S. Lepeshov, R. S. Savelev, D. G. Baranov, and A. Alu, *arXiv preprint arXiv:1703.03159* (2017).
- [31] T. Tanemura, K. C. Balram, D. S. Ly-Gagnon, P. Wahl, J. S. White, M. L. Brongersma, and D. A. Miller, *Nano Letters* **11**(7), 2693–2698 (2011).
- [32] L. Li, T. Li, S. Wang, S. Zhu, and X. Zhang, *Nano Letters* **11**(10), 4357–4361 (2011).
- [33] J. Lin, J. B. Mueller, Q. Wang, G. Yuan, N. Antoniou, X. C. Yuan, and F. Capasso, *Science* **340**(6130), 331–334 (2013).
- [34] J. S. Liu, R. A. Pala, F. Afshinmanesh, W. Cai, and M. L. Brongersma, *Nature Communications* **2**, 525 (2011).
- [35] S. Y. Lee, H. Yun, Y. Lee, and B. Lee, *Laser & Photonics Reviews* **8**(5), 777–784 (2014).
- [36] R. Guo, M. Decker, F. Setzpfandt, I. Staude, D. N. Neshev, and Y. S. Kivshar, *Nano Letters* **15**(5), 3324–3328 (2015).
- [37] C. Lu, Y. C. Liu, X. Hu, H. Yang, and Q. Gong, *Scientific Reports* **6** (2016).
- [38] U. Zywietz, A. B. Evlyukhin, C. Reinhardt, and B. N. Chichkov, *Nature Communications* **5** (2014).
- [39] P. Dmitriev, S. Makarov, V. Milichko, I. Mukhin, A. Gudovskikh, A. Sitnikova, A. Samusev, A. Krasnok, and P. Belov, *Nanoscale* **8**(9), 5043–5048 (2016).
- [40] A. I. Denisov, F. E. Komissarenko, and I. S. Mukhin, *Microelectronic Engineering* **121**, 15–18 (2014).
- [41] B. Hecht, H. Bielefeldt, L. Novotny, Y. Inoué, and D. Pohl, *Physical Review Letters* **77**(9), 1889 (1996).
- [42] A. Drezet, A. Hohenau, D. Koller, A. Stepanov, H. Ditlbacher, B. Steinberger, F. Aussenegg, A. Leitner, and J. Krenn, *Materials Science and Engineering: B* **149**(3), 220–229 (2008).
- [43] D. G. Zhang, X. Yuan, and A. Bouhelier, *Applied Optics* **49**(5), 875–879 (2010).

- [44] S. Frisbie, C. Regan, A. Krishnan, C. Chesnutt, J. Ajimo, A. Bernussi, and L. G. de Peralta, *Optics Communications* **283**(24), 5255–5260 (2010).
- [45] A. E. Miroshnichenko, A. B. Evlyukhin, Y. S. Kivshar, and B. N. Chichkov, *ACS Photonics* **2**(10), 1423–1428 (2015).
- [46] A. Evlyukhin and S. Bozhevolnyi, *Physical Review B* **71**(13), 134304 (2005).
- [47] I. Sinev, I. Iorsh, A. Bogdanov, D. Permyakov, F. Komissarenko, I. Mukhin, A. Samusev, V. Valuckas, A. I. Kuznetsov, B. S. Luk'yanchuk, A. E. Miroshnichenko, and Y. S. Kivshar, *Laser & Photonics Reviews* **10**(5), 799–806 (2016).
- [48] M. Kerker, D. S. Wang, and C. Giles, *JOSA* **73**(6), 765–767 (1983).
- [49] B. García-Cámara, R. A. de La Osa, J. Saiz, F. González, and F. Moreno, *Optics Letters* **36**(5), 728–730 (2011).
- [50] Q. Wang, E. T. Rogers, B. Gholipour, C. M. Wang, G. Yuan, J. Teng, and N. I. Zheludev, *Nature Photonics* **10**(1), 60 (2016).
- [51] T. J. Cui, M. Q. Qi, X. Wan, J. Zhao, and Q. Cheng, *Light: Science & Applications* **3**, e218 (2014).
- [52] P. B. Johnson and R. W. Christy, *Physical Review B* **6**, 4370–4379 (1972).